



**National
Oceanography Centre**
NATURAL ENVIRONMENT RESEARCH COUNCIL

National Oceanography Centre

Research & Consultancy Report No. 55

A comparison of sea surface temperatures in the
Equatorial Pacific Nino regions with results from
two early runs of the NEMO 1/12° Ocean Model

D J Webb

2016

National Oceanography Centre, Southampton
University of Southampton Waterfront Campus
European Way
Southampton
Hants SO14 3ZH UK

^aAuthor contact details:
Tel: +44 (0)23 8059 6498
Email: djw@noc.ac.uk

DOCUMENT DATA SHEET

<i>AUTHOR</i> WEBB, D J	<i>PUBLICATION DATE</i> 2016
<i>TITLE</i> A comparison of sea surface temperatures in the Equatorial Pacific Nino regions with results from two early runs of the NEMO 1/12° Ocean Model.	
<i>REFERENCE</i> Southampton, UK: National Oceanography Centre, 31pp. (National Oceanography Centre Research and Consultancy Report, No. 55)	
<i>ABSTRACT</i> <p>Sea surface temperature observations from the Nino regions of the Tropical Pacific are compared with results from two 1/12° runs of the NEMO global ocean model. The results show good agreement between the model and observations.</p> <p>There was some concern that the model surface temperatures were being strongly coupled to the actual temperatures via the surface boundary conditions. The near surface structure of the ocean was investigated, as were the individual surface flux terms, but no evidence of strong coupling was found. In fact during the strongest warming periods the surface boundary conditions cooled the ocean more than normal.</p>	
<i>KEYWORDS:</i>	
<i>ISSUING ORGANISATION</i> National Oceanography Centre University of Southampton Waterfront Campus European Way Southampton SO14 3ZH UK	
<i>PDF available at http://nora.nerc.ac.uk/</i>	

Page intentionally left blank

A Comparison of Sea Surface Temperatures in the Equatorial Pacific Nino Regions with Results from Two Early Runs of the NEMO 1/12° Ocean Model.

David J. Webb

National Oceanography Centre, Southampton SO14 3ZH, U.K.

Correspondence to: D.J.Webb (djw@noc.ac.uk)

Abstract.

Sea surface temperature observations from the Nino regions of the Tropical Pacific are compared with results from two 1/12° runs of the Nemo global ocean model. The results show good agreement between the model and observations.

There was some concern that the model surface temperatures were being strongly coupled to the actual temperatures via the surface boundary conditions. The near surface structure of the ocean was investigated, as were the individual surface flux terms, but no evidence of strong coupling was found. In fact during the strongest warming periods the surface boundary conditions cooled the ocean more than normal.

1 Introduction

This report forms part of an investigation into the El Nino events in the Tropical Pacific making use of results from high resolution runs of the NEMO global ocean model. Such a study is only worthwhile if we have some confidence that the model behaviour is, in some sense, close to reality.

To this end, this report compares satellite observations of sea surface temperatures (SST) in the Pacific Nino regions with results from the model. As is shown later, the results are encouraging. However the model is forced at the sea surface and, although SST is not itself imposed on the model, it is possible that local surface boundary conditions strongly couple the actual SST values with the model values.

For this reason the study also investigates the net fluxes through the sea surface and the vertical structure of the temperature field. These studies indicate that the model SSTs are not greatly affected by the local surface boundary conditions.

Overall the results imply that it is the large scale dynamical behaviour of the model which is

	Longitude Range	Latitude Range
Nino 1	270° E - 280° E	10° S - 0° S
Nino 3	210° E - 270° E	5° S - 5° N
Nino 3.4	190° E - 240° E	5° S - 5° N
Nino 4	160° E - 210° E	5° S - 5° N

Table 1. The Nino regions of the Equatorial Pacific.

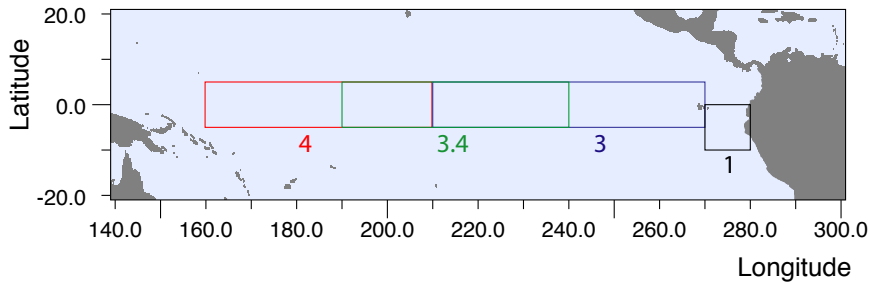


Fig. 1. Locations of Nino regions 1, 3, 3.4 and 4 in the Equatorial Pacific.

primarily responsible for the model’s good SST results. The model may still contain significant errors but on the basis of this study there is no reason not to use the model results to investigate other aspects of the El Nino system in the Pacific.

2 SST Comparisons

2.1 The Nino Regions

Comparisons between model results and observations are made for the four standard El Nino regions. These are specified in Table 1 and illustrated in Fig. 1.

Region Nino 1 represents the area where the El Nino was first identified in the ocean. Warm near surface temperatures there lead to significant reductions in the local fisheries (Wyrтки, 1975).

The other standard Nino regions were introduced when it was realised that the atmospheric response resulted from temperature changes along the equator further west. This is discussed by Trenberth (1997).

Comparisons between model and observations in region Nina 1 should provide a measure of how well the model represents the strong oceanic El Ninos. Similarly comparisons within the other regions, especially Nino 3.4, should provide are a measure of how well it represents the ocean contribution to atmospheric El Nino events.

2.2 Observed Sea Surface Temperatures

The sea surface temperature (SST) values, used for comparison with the model results, are taken from version 4 of the Improved Extended Reconstructed Sea Surface Temperature dataset (ERSST.v4, Huang et al., 2015; Liu et al., 2015) available from the US National Climate Data Center. The dataset is based in ship and buoy observations after they have undergone strict quality control checks and have had biases removed.

Huang et al. (2015) compared the ERSST.v4 results with the earlier ERSST.v3b, with the Hadley Centre Sea Ice and SST dataset (HadISST, Rayner et al. (2003)), with the Centennial Observation Based Estimate of SSTs (COBE-SST, Hirahara et al. (2014)) and, during the period 1997 to 2010, with measurements from the satellite based Along Track Scanning Radiometer (ATSR, Merchant et al. (2015)). The latter is expected to be less affected by clouds than other satellite measurements.

The comparisons show that the different historical datasets are generally in good agreement. Comparisons with the ATSR data show that differences in the mean values are generally below 0.2°C , but with the ERSST.v4 dataset being up to 0.3°C too warm in the cold tongue region of the eastern Equatorial Pacific. The r.m.s differences with the ATSR measurements are about 0.5°C for all three historical datasets but again with the ERSST.v4 value being slightly larger in the cold tongue region.

These ERSST differences on the equator occur east of 120°W (220°E) and so will affect the results in Nino regions 3 and 3.4 discussed later. Close to the South American coast, near 10°S , there is also a region where the mean ERSST value is approximately 0.2°C too cold. This affects part of the Nino 1 region.

2.3 The Nemo Ocean Model

The Nemo model discussed here is one of a family of similar models, all with the same underlying code base, but with different choices of grid resolution and options of representing the underlying physics.

A detailed discussion of the different options is given by Madec (2014). Each option is selected either through a preprocessor flag or through the values of run time parameters. The values used for the two runs discussed here are listed in Appendix 1.

All Nemo ocean models use a horizontal spacing of grid cells based on the Arakawa-C scheme (Arakawa, 1966). For the present runs, tracer points along along the Equator are separated by $1/12^{\circ}$. Off the equator in the Southern Hemisphere, and in the Pacific and Indian Ocean sectors of the Northern Hemisphere, tracer points lie on the same lines of longitude but their separation in latitude is reduced, such that the grid cell surrounding each tracer point remains square.

This arrangement ensures that a finer grid is used at high latitudes where the natural scale of the ocean, the Rossby radius, is also reduced. In the North Atlantic and Arctic, a similar but distorted scheme is used which ensures that the cell sizes do not reduce to zero at the pole.

In the vertical, the model has 72 layers, which range in thickness from 1 m at the surface to 204 m in the lowest layer. The thicknesses are based on an analytic equation involving two tanh functions. This ensures a smooth transition between the strongly stratified surface layers, which need to be well resolved, and the weakly stratified deep ocean, where much thicker layers can be used.

The model uses two time-stepping schemes, one for the slow baroclinic or internal modes of the ocean and a much shorter one for the fast barotropic or external models. The latter includes the tides and the barotropic Rossby and Kelvin waves.

The primary model variables are the ocean potential temperature, its salinity and the two horizontal components of velocity. Vertical velocity is calculated each time step from conservation of water volume. The conservation equations for these variables (for velocities the momentum conservation equations) are stepped forward using the slow time-stepping scheme and with a time-step of 200 seconds.

The second set of variables, the sea surface height SSH (i.e the elevation above the mean), and the two depth integrated components of horizontal velocity are integrated forward using a time-step of 2 seconds. In this case the time-stepping equations are derived from conserving volume or horizontal momentum in each vertical column of water.

The horizontal advection of tracers is modelled using the TVD scheme (Zalesak, 1979). In this scheme the flux of tracer across an interface is given by the product of the water velocity through the interface and the average of the tracer values in the cells on either side of the interface. After all interface fluxes have been calculated, the numerical generation of extreme values is prevented by constraining the new value to lie within the range of values of neighbouring grid boxes. Unfortunately this final step can lead to non-conservation of tracer.

Sub-grid scale horizontal diffusion is represented by a Laplacian (∇^2) operator acting along density surfaces. In the vertical a modification of the turbulent kinetic energy (TKE) scheme is used (Gaspar et al., 1990; Madec, 2014). This parameterizes the turbulence produced by shear at the boundaries and within the ocean.

Momentum is advected horizontally using a scheme designed to conserve both momentum and enstrophy (Madec, 2008). In the vertical, viscosity is represented using the same TKE scheme as the tracers. In the horizontal, the model uses a bi-harmonic (∇^4) operator acting along level surfaces.

2.3.1 Boundary Conditions

The flux of each tracer is set to zero on the side and bottom boundaries of the ocean. In the momentum equations the model uses free-slip, so there is no stress at horizontal boundaries. At the ocean bottom, a stress term is used which depends on the square of the water velocity.

At the surface, fluxes of tracer and momentum are calculated at each timestep using atmospheric data from the ECMWF reanalysis runs (See Appendix 2).

2.3.2 Critique

As this note is concerned with the realism of the model, it is worth briefly discussing possible sources of error. The non-conservation of tracers was mentioned above. The error will not affect regions where velocities are low or the tracer gradients are constant or slowly varying. However it could affect regions where velocities are high if there are also rapid changes in tracer gradient. Thus errors could occur in the boundary currents and equatorial currents.

A second potential error comes from the use of the free slip velocity boundary condition and the bi-harmonic (∇^4) horizontal viscosity. Both approximations were first introduced in low-resolution models to improve the appearance of western boundary currents.

The use of a no-slip condition meant that velocities remained large close to the western boundary. However, in reality, velocities are zero at the boundary and when turbulence mixes this water into the offshore current it has a significant effect on the along-shore pressure gradient.

Bi-harmonic friction was used in the same models, primarily to prevent non-linear instabilities. In all ocean models, turbulence tends to move energy to short wavelengths and, if the energy there is not removed rapidly enough, amplitudes grow exponentially and the model soon becomes unstable. At low resolution the value of Laplacian viscosity required to do this is unphysically large so the bi-harmonic operator was used.

However in high resolution models like this one, physically realistic Laplacian operators representing the effects of sub-grid scale turbulence are possible. Thus in the present case the continued use of a bi-harmonic operator may reduce the amplitude of the shortest waves but leave too much energy at intermediate wavelengths.

All models involve compromises, so this critique should not be taken too seriously, but potential errors need to be kept in mind when studying the model results. In the analysis that follows the main focus is on the heat transport in the model, especially the vertical diffusion of heat. Errors at the boundaries are probably not critical but equatorial currents can be strong, so in this region the advection terms may lead to small errors in the conservation of heat.

3 SST Comparison

The average SST values in the four Nino regions are plotted against the ERSST estimates in Figs. 2 and 3. These show that the model results reproduce many of the features of the observations but that there are noticeable differences.

In the Nino 1 region, both model runs show temperatures that are too warm during the cold period at the end of each year. There is a significant year to year variation but, in Run 1, the errors are largest in the early part of the run and become smaller later. In Run 6 the pattern of errors is similar throughout the run.

The Nino 4 region has much weaker annual signal but there are significant year to year variations.

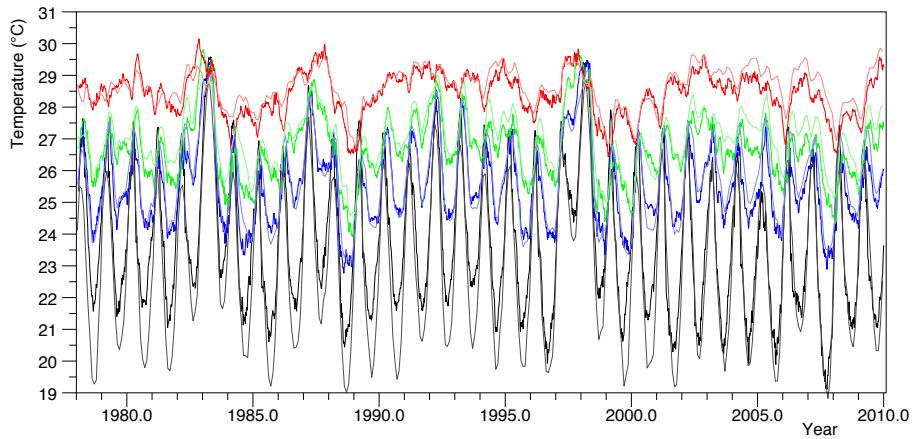


Fig. 2. Observed sea surface temperatures from ERSST Version 4 and results from run 1 of the Nemo model averaged over Niño regions 1 (black), 3 (blue), 3.4 (green) and 4 (red). The model data is plotted in bold colours, the observed data in lighter colours.

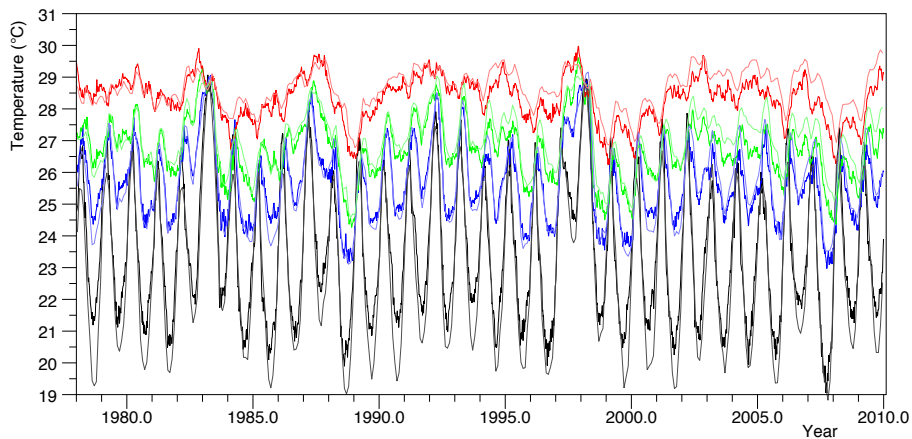


Fig. 3. As figure 2 but for run 6 of the Nemo model

Both model runs track the main changes in SST but, in the decade following the year 2000, run 1 produces SST values which are too cold. Run 6 starts the analysis period too warm but after 1983 it is also often too cold.

As might be expected, regions Niño 3 and 3.4 show an intermediate behaviour. The model results follow the observed annual cycles, the year to year variations in SST and many of the shorter scale features. However again in both runs the model SSTs tend to be too cold, especially towards the end of the analysis period.

One encouraging aspect of the results is the good agreement between the model and observations during the strong El Niños of 1982-83 and 1997-98. In each of the cases warm SSTs are first found in the west and the signal propagates eastward until similar temperatures are found in all four Niño

Region	Observed Average	r.m.s.	Run1 Offset	r.m.s.	Run 6 Offset	r.m.s.
Nino 1	22.98	2.40	+0.70	0.33	0.49	0.45
Nino 3	25.74	1.30	-0.16	0.38	-0.05	0.39
Nino 3.4	27.03	0.94	-0.31	0.19	-0.26	0.19
Nino 4	28.62	0.61	-0.18	0.24	-0.27	0.19

Table 2. Averaged and r.m.s. variation in the observed temperature ($^{\circ}\text{C}$) for the four Nino regions during the period January 1978 to December 2009, together with the model offsets and the model r.m.s variance after applying the offset.

regions.

Average temperatures, the model offsets and the root mean square of the differences for the different regions and runs are given in Table 2. The tabulated values confirm that average model temperatures are too warm in the Nino 1 region and are too cold in the three other regions. After the offsets have been removed the r.m.s. differences between the model and observations are 0.5°C and 0.7°C in the Nino 1 region and between 0.1°C and 0.4°C in the other three regions.

Overall the results show that there are some small systematic differences with the ERSST dataset but otherwise the model appears to be good at representing the year to year changes in SST and many features at shorter timescales. In fact the main concern coming from this analysis is that the agreement may be too good, indicating that the model SSTs are being forced towards the correct values. This cannot be done directly because, unlike the salinity field, there is no near surface relaxation term forcing the model towards the observed values.

However the surface flux of heat in and out of the ocean does depend on the air temperature in contact with the ocean and, as this depends largely on the actual sea surface temperature, it is inevitable that some feedback is involved. This could be a small term in the heat flux equation or it could be dominant. As a result, all that can be concluded from the SST comparisons is that the model has no major fault. Before it can be used with confidence to study other aspects of the system, further tests are necessary.

3.1 Behaviour at Depth

If the model response in the El Nino regions is dominated by the surface heat fluxes, then this might be expected to show up in the temperatures just below the ocean surface. Periods of heating might then generate a shallow thermocline. Similarly periods of cooling might result in a rapid deepening of the mixed layer.

If instead the SST values are dominated by advection of warm water from elsewhere or to the propagation of large scale internal waves, then temperature changes should involve a large number of layers with no indication of a downward propagating signal.

To help investigate this, the near surface temperatures in Nino regions 1 and 3.4 during the period

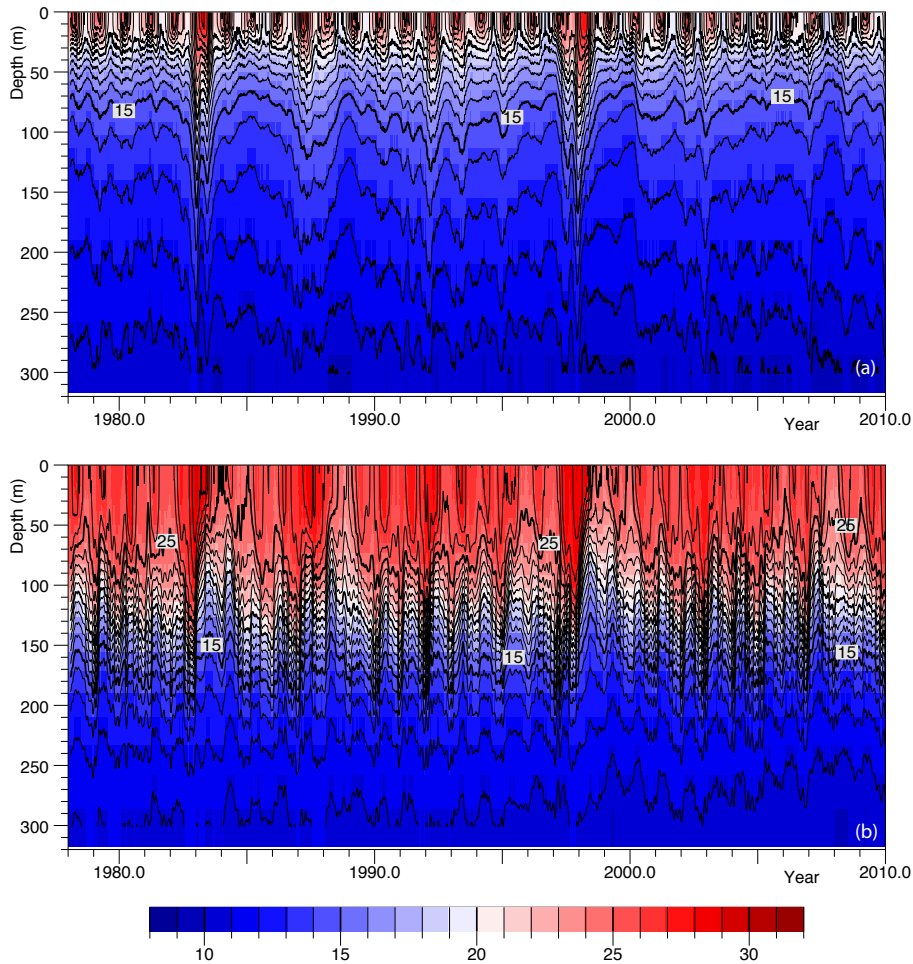


Fig. 4. Average temperatures ($^{\circ}\text{C}$) in the near surface during Run 1 of the model, for (a) the Nino 1 and (b) the Nino 3.4 regions, plotted as a function of time and depth.

1978 to 2010 are shown in Fig. 4 for run 1 and Fig. 5 for run 6. In both of the runs the Nino 1 region shows large annual temperature changes in the top 20 m but in many years this is only weakly correlated with changes below 100 m. In contrast during the El Ninos of 1982-83 and 1997-98 the rise in SST is correlated with temperature increases at all levels down to 200 m and beyond.

A clearer picture of the model response is given in Fig 6 which, for run 6, shows just the period from the start of 1980 to the end of 1984. If for the moment we ignore the El Nino of 1983, then in the Nino 1 region, SSTs increase around the turn of the year but the warming does not extend beyond a depth of 30 m. Warmest temperatures occur around March and affect only the top 10 m of the ocean. There is then a period of cooling during which the surface mixed layer deepens to 20 m or more.

During the period of surface temperature increase, levels below 50 m appear uncorrelated, except

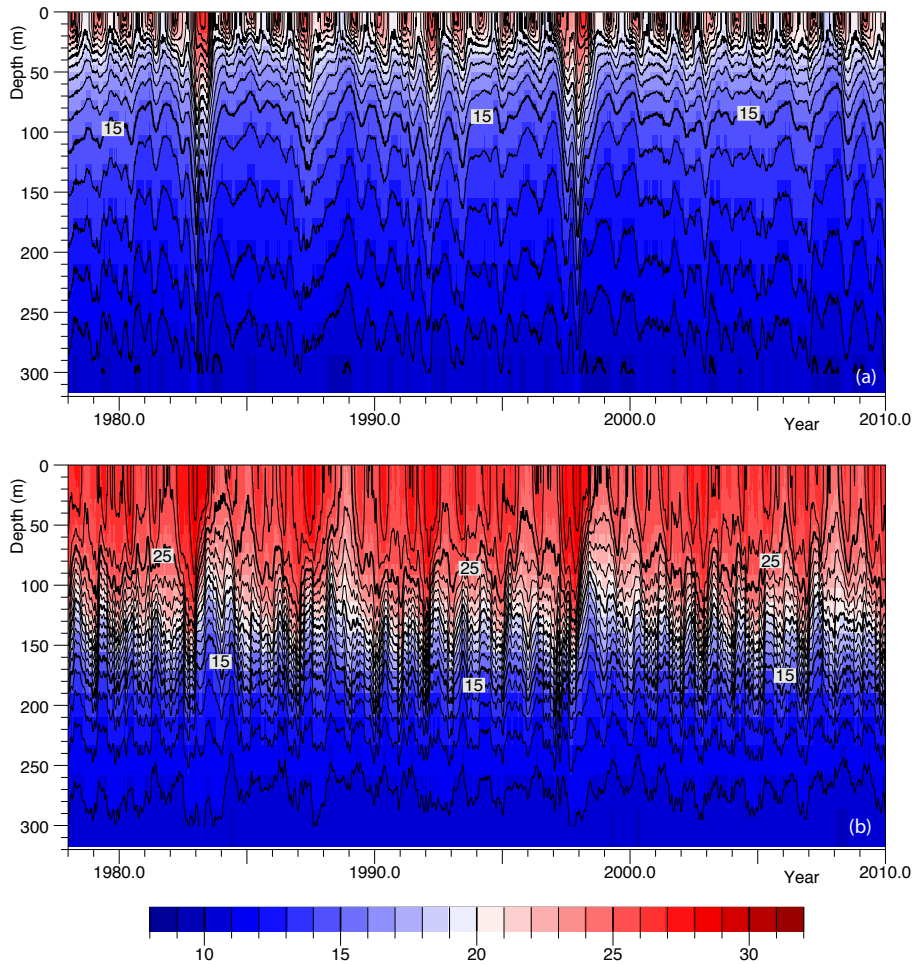


Fig. 5. Average temperatures ($^{\circ}\text{C}$) in the near surface during Run 6 of the model, for (a) the Nino 1 and (b) the Nino 3.4 regions, plotted as a function of time and depth.

possibly in 1983. However at the time when SST temperatures start to fall, temperatures at all depths below 20 m start to increase. The temperatures reach a maximum at all depths around the middle of the year, after which they start to fall back to near their original values.

During the 1982-1983 El Nino, an increase in SST occurs as normal at the turn of the year, but now the increase extends below 250 m. During the early part of the year, SST increases, but below 30 m the ocean cools. There is then another period of deep warming later in the year but this time it occurs well below the (delayed) period of surface cooling.

The patterns of behaviour in the Nino 3.5 region are less clear. The annual SST signal in the Nino 3.5 region has a range of approximately 3°C , which is less than the 5°C seen in Nino 1. The main surface thermocline lies near 150 m, whereas in Nino 1 it was around 20 m. In Nino 3.5 the annual signal in SST has a range of approximately 3°C compared to 5°C in Nino 1. The warming is

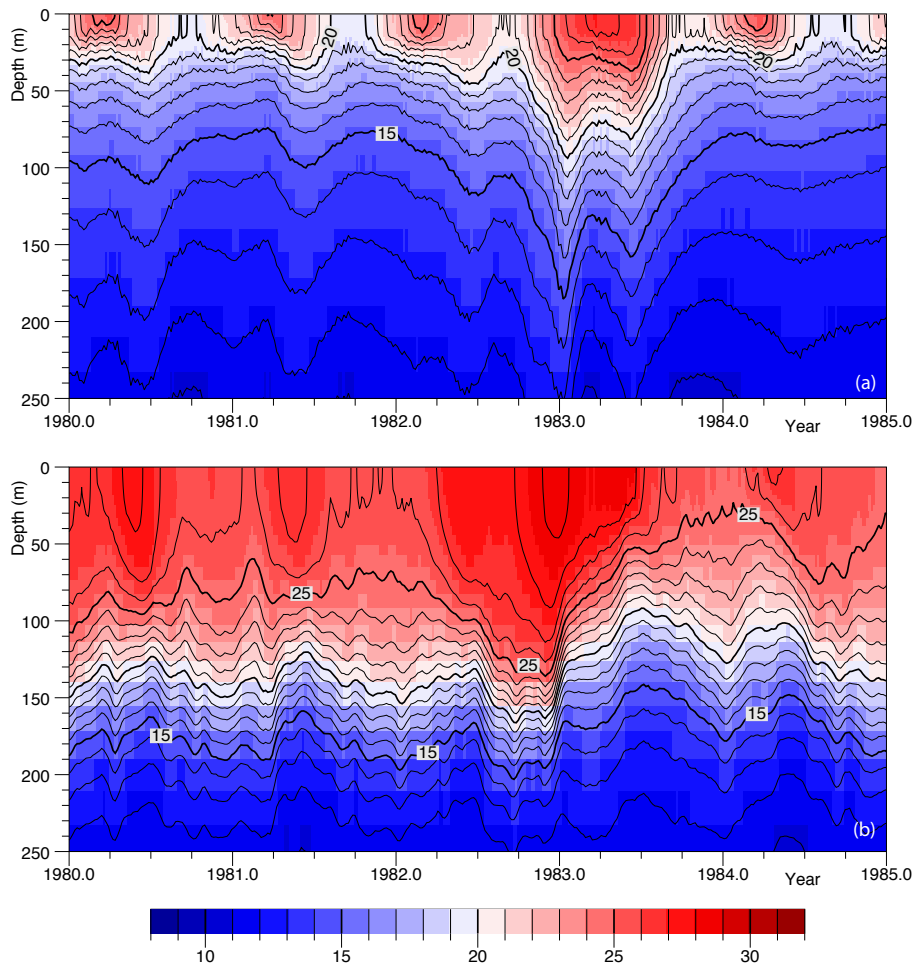


Fig. 6. The period 1980 to 1985 from Fig. 5

greatest around May and extends to depths of approximately 100 m, i.e. above the main thermocline. The thermocline itself rises during the period of warming such that temperatures at 200 m are coolest at the time the surface is warmest.

The behaviour during the 1982-83 El Niño shows significant changes. In early 1982 the surface warms and the deeper layers cool, as in a normal year, but then the surface layers stay warm and the thermocline, after dropping rapidly, stays deeper than usual until the end of the year.

This time the largest surface temperatures occur around the beginning of 1983 after which they slowly drop until a minimum is reached a year later. The beginning of 1983 is also a time when the thermocline shallows rapidly and it remains shallower than normal until late in the year when it deepens, again reaching a maximum when the surface temperatures are a maximum.

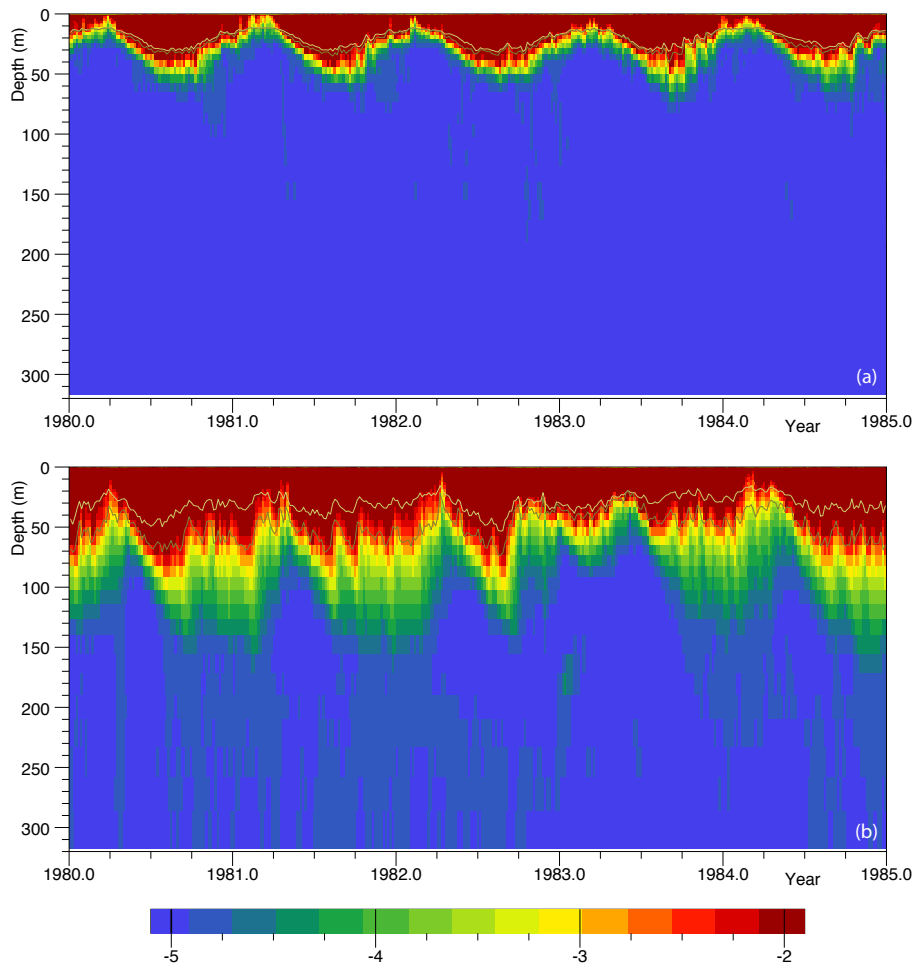


Fig. 7. Average value of the base 10 log of the Vertical Diffusion Coefficient in Nino regions 1 and 3.4 also showing the depth of the mixed layer (black) and turbocline (light brown).

3.2 Interpretation

In order to understand the above results we need to consider the physical processes that might be responsible. The first of these is the direct effect of surface heating and cooling. This will have most effect of the surface mixed layer and is almost certainly responsible for the annual cycle of heating and cooling seen of the top 20 m of the Nino 1 region (See fig 6).

Two other obvious processes are the effects of advection and the passage of long equatorial waves, especially internal Kelvin and Yanai waves. Figs. 3 to 6, all show coherent vertical movements of the thermocline which could be due to either process. When there is no change in surface temperature then wave propagation is the most likely candidate. However if SST changes as well, especially when this occurs outside the normal seasonal pattern, as in the Nino 3.5 region in late 1982, then advection is most likely.

Other mechanisms to consider are less direct. In Nino 1, the shallowing of the thermocline early in the year could be responsible for a greater heating of the surface mixed layer in the following months. Also in the Nino 1 region, if storms are associated with the mid-year surface cooling, these could increase the amount of turbulence in the top layers of the ocean. The effect could partly explain the cooling of the surface layer during this period and explain the warming of the deeper layers. Such warming of the deep layers is not seen (or at least is not obvious) in the Nino 3.5 region, so it is unlikely advection or wave propagation from this region is responsible for the warming of the Nino 1 region.

Finally there is the El Nino mechanism itself. This is likely to be responsible for many of the features seen only during the 1982-83 period. In particular, if the warm temperatures in the Nino 3.5 region in late 1982 and early 1983 are responsible for lighter winds in the Nino 1 region, this may explain the warmer Nino 1 SST in early 1993.

In terms of the model performance, if the SST values discussed here are primarily a response to local surface forcing then, although the comparisons between the model SSTs and observations are promising, the representation of other processes in the ocean could be in considerable error. However if there are periods when surface forcing is not dominant but the comparison is still good then there is some justification in thinking that the other key physical processes are being represented reasonably well.

The final section of this report is thus concerned with investigating the fluxes in and out of the Nino regions to see if they are all dominated by surface fluxes or whether other processes are having a significant impact.

4 Heat Content and the Surface Heat Flux

In the NEMO model the heat content of a volume of ocean is given by the equation,

$$H = \int \rho T(x,y,z) dz dy dz. \quad (1)$$

where H is the heat content, T temperature and ρ is the specific heat. In the model this has the constant value $4.0 \times 10^6 \text{ J m}^{-3}$.

Figure 8a shows the heat content of the Nino 1 region between the surface and depths of 15, 65, 190 and 537 m. in units of Giga-Joules per square metre of surface area. The data is from run 6 of the Nemo model and covers the same period as Fig. 6.

The rate of change in time of the heat content per unit area is shown in Fig.8b, the deeper colours corresponding to deeper layers. The data is plotted in this manner so that the changes can be compared with the heat gain or loss through the ocean surface, shown in red. This shows that within the Nino 1 region the surface flux acts to heat the ocean.

The figure also shows that during periods of heating the surface flux is often similar to or greater

than the rate of change of heat content of the underlying ocean. This implies that water is being warmed as it is passing through the region, a result consistent with the expected upwelling near the equator and the warming of Humboldt Current water as it travels through the region.

Although the mean annual heat content signal may be explained by changes in the surface heat flux, there are also large short period changes which cannot be explained in this way. Many of these have periods of a month or less and may be due to oceanic wave motions passing through the region or the movement of nearby Tropical Instability Waves.

In the period 1980 to 1983, there also appears to be a semi-annual signal. This starts with a relatively weak cooling of the ocean in January, a stronger warming around April, a strong cooling around June and a weaker warming in the Autumn. Although the cooling in June coincides with the minimum downward heat flux at the surface there is no other evidence that the two are connected.

However the main feature in both Figs.8a and 8b are the large changes in heat content associated with the time of the 1982-83 El Nino. As these are up to an order of magnitude larger than the heat flux through the ocean surface, there is no way that the imposed surface fluxes can be controlling the deep temperature field in the model.

Figures 9a and 9b, show the comparable results for Nemo region 3.4. The surface flux shows a small seasonal signal which, except for the 1982-1983 El Nino, has a maximum in the early part of each year. This is reflected weakly in the heat content of the ocean above 65 m but not in the deeper layers.

5 The Surface Heat Flux Components

The surface heat flux subroutines used in these model runs are based on the bulk formula proposed by Large and Yeager (2004). In terms of the physics four main terms are involved. These are the short wave radiation from the sun, the sensible heat flux due to the contact between the ocean and atmosphere, the long wave radiation exchange between the ocean and atmosphere and finally the latent heat flux due to evaporation from the ocean surface.

The fluxes depend on the atmospheric forcing data, which is based on observations, and on the model SST values. Details are given in Appendix 2.

If we consider first the shortwave radiation flux, this is the top of the atmosphere value due to the sun, reduced to allow for the sun's angle and the effects of clouds and aerosols. The model SST is not involved and neither is the actual SST, except weakly through its influence on generating clouds and forming marine aerosols. As increased SST is likely to produce more convection, and thus more clouds and aerosols, in this case the feedback is likely to be negative.

The equation used for the sensible heat flux involves the temperature difference between the model SST and the temperature of lowest atmospheric layer. In reality the latter is tightly coupled to the actual SST and so, through this term, the model SST might be positively coupled to the actual SST.

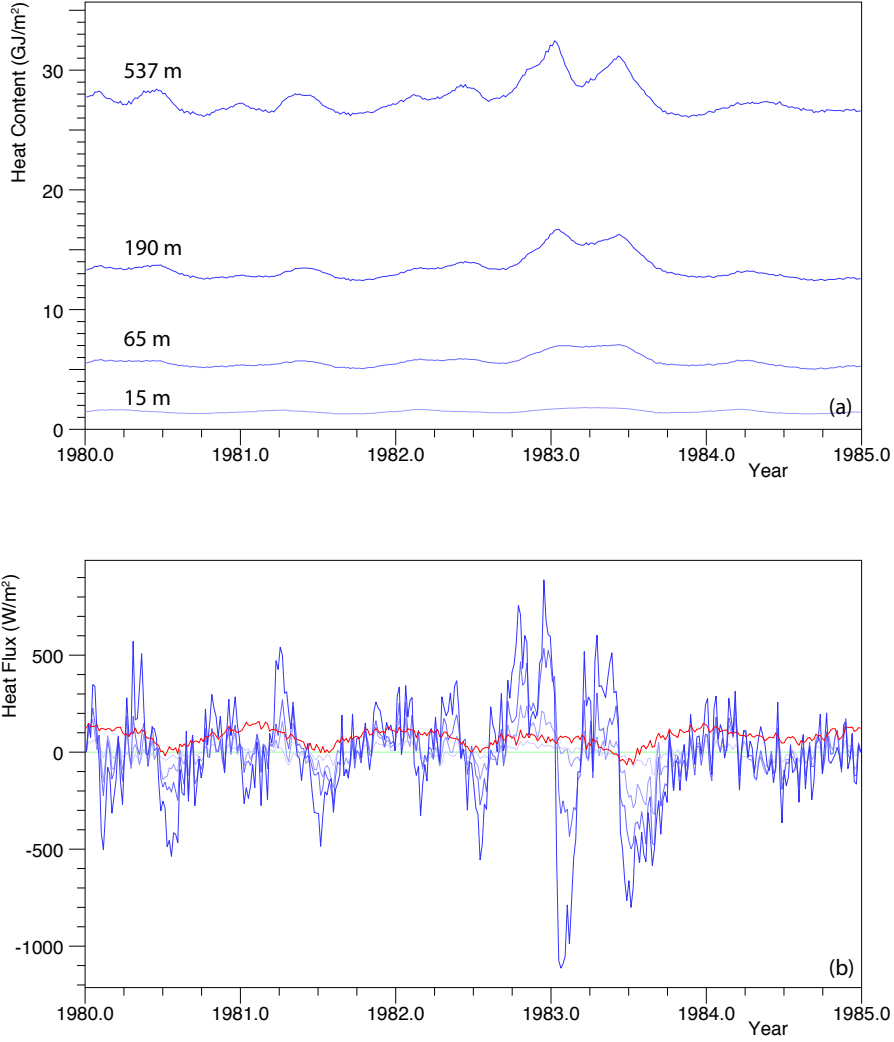


Fig. 8. Figure (a) shows the heat content of Nemo region 1, integrated between the surface and depths of 15, 65, 190 and 537 m as a function of time and represented as Giga Joules (GJ) per unit surface area. (b) The rate of change of heat content for the same set of model volumes and represented as Watts per unit surface area. Light blue represents the shallowest box, darker blues correspond in sequence to deeper boxes. The red line is the heat gain through the ocean surface.

The effect of the sea surface temperatures on the long wave radiation term is a bit more subtle. The upwards radiation out of the ocean is given by the black body radiation equation for material at the temperature of the sea surface. This is,

$$F_{ro} = S_B T_o^4 \quad (2)$$

where F_{ro} is the upward long wave radiation from the ocean, T_o the model sea surface temperature

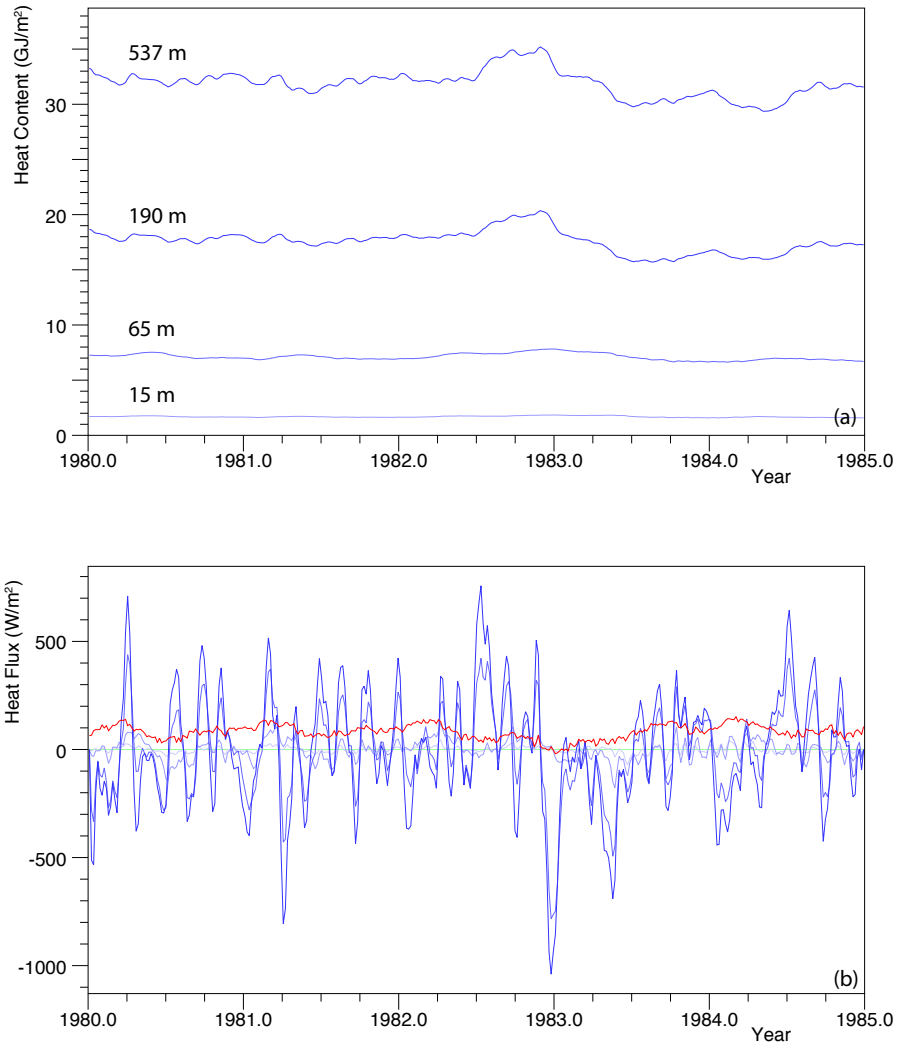


Fig. 9. (a) The heat content of Nemo region 3.4, integrated between the surface and depths of 15, 65, 190 and 537 m as a function of time and represented as Giga Joules (GJ) per unit surface area. (b) The rate of change of heat content for the same set of model volumes and represented as Watts per unit surface area. Light blue represents the shallowest box, darker blues correspond in sequence to deeper boxes. The red line is the heat gain through the ocean surface.

and S_B the Stephan-Boltzmann constant.

At long wavelengths the atmosphere appears foggy, i.e. radiation only travels a limited distance. As a result, the downward flux at the sea surface is an integral over contributions from a range of atmospheric levels. Most of the radiation comes from the lowest layers of the atmosphere but some comes from higher cooler layers. As a result the effective temperature of the downward atmospheric flux is usually somewhat less than the temperature of air in contact with the sea surface.

This means that the net flux is usually upwards from ocean to atmosphere. However as the near

surface atmospheric temperatures are still important and as these are forced by the actual SST values, the model SST may again be positively coupled to the actual SST.

Finally, the latent heat flux, which cools the ocean, depends on the difference between the specific humidity of the lowest atmospheric layer and the saturated value for air at the temperature of the sea surface. The specific humidity is defined as kilograms of water per kilogram of atmosphere. The saturated value is strongly dependent on the model SST value but as the difference in specific humidity does not depend on air temperature there is no direct feedback from the actual sea temperature.

However if the model SST is lower than actual value, this reduces the difference between the observed air humidity and the saturated value based on the model SST. This then reduces the amount of evaporation in the model, reduce the latent heat cooling and so again increase the model SST.

In principal therefor, for each of the four flux terms, changes in the actual SST values may have a feedback effect on the model SST. For the shortwave radiation this is likely to be a negative feedback, increases in actual SST leading to a reduction in ocean surface heating. However in the other three cases, a positive feedback is likely, an increase in actual SST leading through the flux terms to an increase in model SST.

If these positive feedbacks are strong enough then it is possible that that apparent good agreement between the model SST values and observations is not a result of a good model but just a measure of the strength of the feedbacks. In the next section the fluxes are investigated in model detail to see if there is any evidence for this.

6 Air-Sea Temperature Differences

Figure 10 shows the average sea surface temperature in the Nemo 1 region during the period 1980.0 to 1985.0. The period includes a series of reasonably typical years plus the El Nino period, of late 1982 and early 1983, and the following La Nina. Except for very short periods, the ocean temperature is above that of the atmosphere so, as is the case over much of the ocean (Large and Yeager, 2004), the sensible heat flux is usually from ocean to atmosphere.

The temperature fields are highly correlated, being highest in the spring months and lowest in the autumn. If the ocean is responding to atmospheric forcing then one might expect the air temperature to lead the oceanic response. There is some evidence for this in 1981, the temperature difference being smallest during the warming period and larger when the system is cooling. However in other years, the temperature difference is often lower than normal in both the warming and cooling periods.

During the El Nino period of 1983, when sea surface temperatures are largest, the average air-sea temperature difference is much larger than in the other years. This means that, at least as far as the sensible heat flux is concerned, the atmospheric forcing cannot be controlling the sea surface temperatures. Thus the good agreement between model and observations (Fig. 2) seen during the El Nino cannot be due to this mechanism.

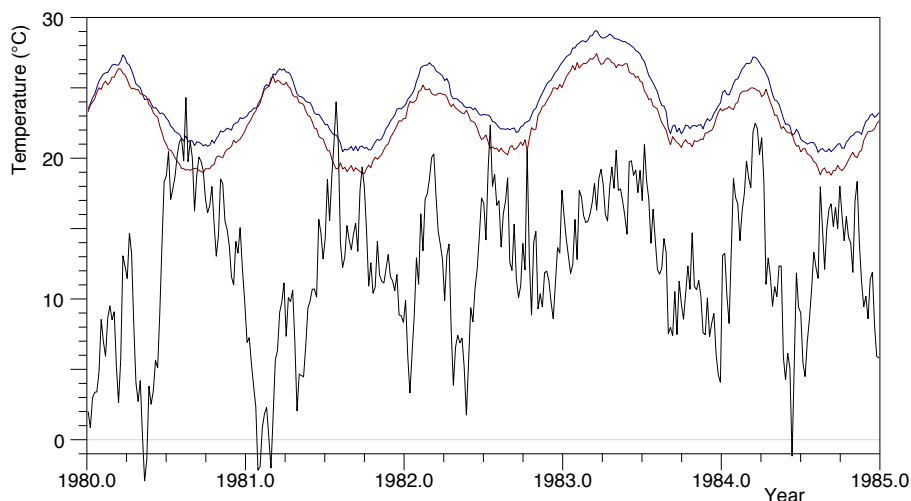


Fig. 10. Average temperatures of the sea surface (blue) and atmosphere (red), in the Nino 1 region during the period 1980.0 to 1985.0. The sea surface temperature, averaged over 5 days, is from the NEMO model. The atmospheric temperature is from the ECMWF reanalysis used to force the model. The back curve is the difference multiplied by ten.

However it is possible that other flux terms are involved. These are considered in the next section.

7 Changes in the Flux terms

Figure 11 shows a more detailed set of surface heat flux components averaged over the Nino 1 region for the period 1980.0 to 1985.0.

The atmospheric data used to force the model is available as three hourly or one day averages, depending on the field. It includes the short wave flux incident on the ocean but none of the other flux components. The ocean model is only available as five-day averages. It includes the incident short wave flux and total heat flux but again has none of the other flux components.

Estimates of the Sensible, Long Wave and Latent Heat fluxes were obtained by first interpolating the atmospheric fields onto the oceanic grid and then averaging them over the same five day interval as the ocean model. Off-line versions of the Nemo model routines implementing the Large and Yeager (2004) CORE surface flux scheme, were then used to calculate the fluxes at the sea surface for the five-day periods.

7.1 Comparison with Model Total Heat Flux

Because the present method misses the effects of the diurnal cycle and any other process with a time scale of less than five days, it is instructive to first compare the total heat flux calculated by the model with that calculated by the present method.

The model result is shown as curve (e) in the figure and the calculated result as curve (f). The

difference is plotted as curve (g). The curves show that there is a small difference between the two calculations, but it is fairly constant and does not differ significantly from normal during either the El Nino or La Nina periods.

7.2 Short Wave Radiation

Figure 11 shows that the short wave radiation due to the sun entering the ocean has an average value of around 190 Wm^{-2} . This is a maximum around the beginning and end of each year and a minimum in the middle of each year. Although this is consistent with a seasonal signal, the Nino 1 region is only just south of the equator and so another factor such as cloudiness is probably involved.

It is also noticeable that during the first few months of 1983, during the El Nino, the incoming short wave radiation is much weaker than normal. As the El Nino is associated with increased convection in the Eastern Pacific, it is likely that this is also a result of increased cloudiness. It also means that the high model temperatures during the El Nino period are not a result of increased incoming solar radiation.

7.3 Long Wave Radiation

The figure shows that the long wave fluxes, out of and into the ocean, have values between 390 and 480 W/m^2 . The outgoing radiation shows a behaviour similar to that of sea surface temperature (Fig. 10), which is to be expected as it is the black body radiation of the ocean surface. The downward flux is noisier than that of the atmospheric temperature at 2 m., a reflection of the fact that it includes contributions from clouds and higher layers of the atmosphere.

The sum of the two fluxes, show a loss from the ocean of between 20 and 40 Wm^{-2} . In most years this is greatest when sea surface temperatures are large, implying that high sea surface temperatures are unlikely to be forced by the long wave radiation from the atmosphere. However during 1993, although the ocean is warmer than normal, the heat loss stays around 30 Wm^{-2} , so the increased atmospheric long wave input during this period could be a contributing factor.

7.4 Sensible Heat Flux

Figure 10 shows that during the period studied, the sensible heat flux loss from the ocean lies between 0 and 20 Wm^{-2} . Although the original concern was that the model sea surface temperature values were being forced by the air temperature, this shows that the sensible heat flux smallest of the four main terms.

Lowest values for sensible heat loss are found during the early months of 1980, 1981 and 1982, when the ocean is warmest. It is thus possible that the atmospheric temperature field is forcing the sea surface temperature in the right direction to agree with observations during this period, but the change in flux is so small that it is unlikely to have a significant effect.

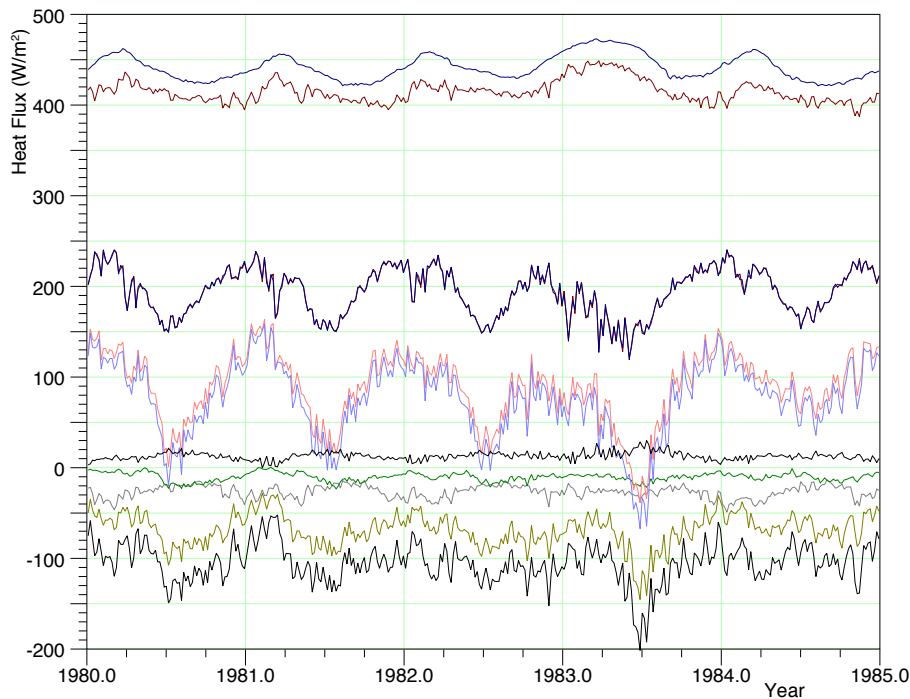


Fig. 11. The surface heat fluxes of the Niño 1 region during the period 1980.0 to 1985.0 in units of W/m^2 . Starting from the top (a) (blue) Outgoing ocean Long Wave radiation, (b) (brown) Incident Long Wave atmospheric radiation, (c) (black) Incident Short Wave solar radiation, (d) (pink) Net flux into ocean (model output), (e) (light blue) Net flux into model (calculated here), (f) (black) Difference between model output and this calculation, (g) (green) Sensible heat flux into ocean, (h) (grey) Net Long Wave flux into ocean, (i) (green-brown) Latent heat flux into ocean, (j) (black) Sum of Sensible, Long Wave and Latent fluxes.

7.5 Latent Heat Flux

The results show that this is the largest of the terms whose magnitude involves both the ocean and atmosphere. The resulting heat loss from the ocean lies between 50 and $150 W m^{-2}$ with some of the largest heat flux loss coinciding with periods when the Short Wave flux is a minimum and the ocean surface is cooling. There appears to be a correlation between the periods of minimum latent heat loss and warmest sea surface temperatures but the effect is weak and may instead reflect a response to the maximum short wave flux at these times.

7.6 Total Forcing

Overall the results indicate there may be a small amount of feedback from the actual sea surface temperature, via the resting atmospheric temperature, back to the model sea surface temperature. However the results also indicate that any such feedback is small compared with the changes in the incoming shortwave radiation or the cooling often produced by the latent heat term when sea surface temperatures are high.

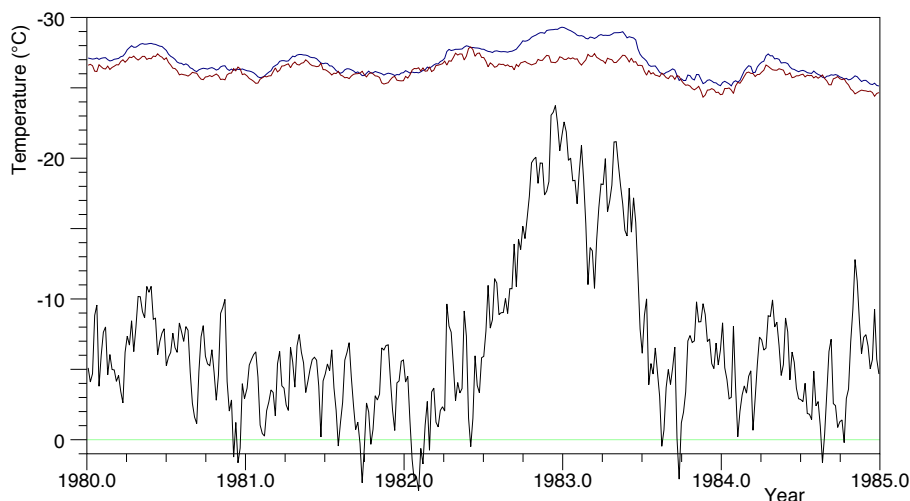


Fig. 12. Average temperatures of the sea surface (blue) and atmosphere (red), in the Nino 3.4 region during the period 1980.0 to 1985.0. The sea surface temperature, averaged over 5 days, is from the NEMO model. The atmospheric temperature is from the ECMWF reanalysis used to force the model. The back curve is the difference multiplied by ten.

Although a negative cannot ever really be proven, the results indicate that in the Nino 1 region, the sea surface temperatures are not being controlled by any feedback terms. In particular it is noticeable that in the periods prior to and during the strong El Nino of 1982-83, the net heat influx into the ocean is significantly less than in other years.

This indicates that the high model sea surface temperatures seen during the El Nino were not due to local forcing by the atmosphere. Instead they must be due to the ocean model physics.

One possibility is that the El Nino temperature maximum was due to equatorial Kelvin or Yanai waves. However although a simple wave motion might be responsible for the increase in the thickness of the warmest near-surface layers, seen in Fig. 6, it would not produce the increases in sea surface temperature seen in the same figure.

The alternative is that the warm temperatures are due to advection by the model and the processes that determine the temperature of the advected water are being represented well by the model. Thus although this part of the analysis was carried out in order to find faults in the previous analysis, the results provide further evidence for how well the model represents all of the processes contributing to an El Nino.

8 The Nino 3.4 region

Figures 12 and 13 are the corresponding figures for the Nino 3.4 region in the Central Equatorial Pacific. In this case the sea and air temperatures are much closer than in the Nemo 1 region, the exception being the El Nino period of 1982-83.

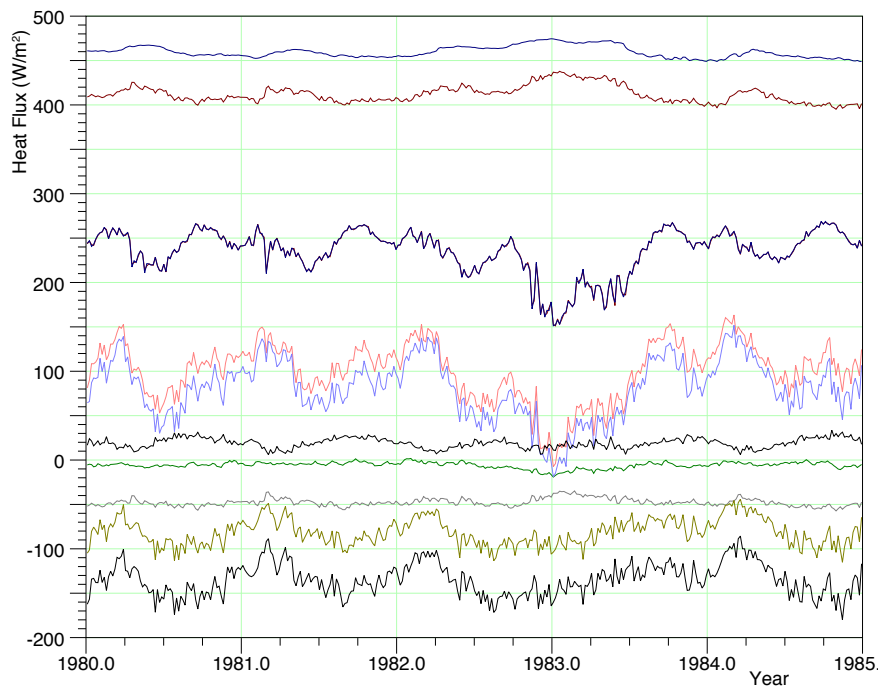


Fig. 13. The surface heat fluxes of the Niño 3.4 region during the period 1980.0 to 1985.0 in units of W/m^2 . Definition of the fluxes as in Fig. 11.

The sensible, long wave and latent heat fluxes have similar magnitudes to those in the Niño 1 region, the main change being a slight increase in the long wave flux out of the ocean. The variability of all three fluxes is much reduced, but again the latent heat loss increases rapidly during the period that the El Niño is developing. The total net heat flux into the ocean is also a minimum during this period.

The implications are similar to those coming from the Nemo 1 results. Thus there is little evidence that feedbacks are responsible for the good agreement between the model and observations seen in Figs. 2 and 3. Instead the good agreements between the model and observations during the El Niño indicate that the model is performing well.

9 Conclusions

The comparisons between model sea surface temperatures and observations indicate that the NEMO model is performing well in all of the El Niño regions studied. However there was a concern that the apparent good agreement might be a result of a feedback involving the original sea surface temperatures and the atmospheric fields used to calculate the model surface fluxes. The model may also have developed a thin near surface layer which responded rapidly to such feedbacks

The vertical structure of the ocean was investigated and it was found that no thin layer developed

other than that seen in the Nemo 1 region associated with the the normal seasonal cycle.

The surface fluxes were also investigated to see if there was any evidence of feedback. The results showed that if it existed such a feedback was small and swamped by changes in the incoming solar radiation and the latent heat flux. It was also found that at the start of and during the main El Nino warming period changes in these terms resulted in a much greater cooling of the ocean.

The main conclusion of the study is therefor that the NEMO ocean model is performing well in the Equatorial Pacific Ocean. The results also indicate that advection has a key role in increasing sea surface temperatures during an EL Nino and that simple Equatorial Kelvin or Yanai waves are not involved.

Acknowledgements. I wish to acknowledge the role of Dr A Coward who carried out the model runs and who provided advice and help in the analysis of the output. I also wish to acknowledge the support of NERC, the UK Natural Environment Research Council, both directly and through the Marine Systems Modelling group at the National Oceanography Centre. The MSM group provided essential material support for this research and funded publication of the results.

Appendix 1. Model Specification

Because of the large number of options available for the NEMO program, the full specification of the model used for a particular study requires the NEMO version number, the preprocessor flags used when compiling the code and the run time parameters read by the model at the start of each run.

In the present case the model specifications for the two runs are identical. The base code for Run 1 was NEMO version 3.4, for run 6 it was 3.5¹.

The preprocessor flags are:

key_orca_r12=75	1/12°model with 75 levels.
key_dtatem	Initial temperature field from Levitus seasonal data set.
key_dtasal	Initial salinity field from Levitus seasonal data set.
key_dynspg_ft	Use filtered form of free surface code.
key_ldfslp	Use free slip horizontal boundary condition.
key_traldf_c2d	Horizontal diffusion term function of grid size.
key_dynldf_c2d	Horizontal viscosity term function of grid size.
key_zdftke	Turbulent Eddy Kinetic Energy dependent vertical diffusion.
key_tradmp	Relaxation to Levitus in some geographical regions.
key_mpp_mpi	Use massively parallel version of code.
key_netcdf4	Use netcdf compression and chunking.
key_lim2	Ice model flag.
key_lim2_vp	Ice model flag.
key_vvl	Co-ordinates move relative to ocean surface.

The model parameters are:

nn.leapy=0 No extra day in leap years.

¹I understand that the version change did not change the physics of the two runs

ln_zps = .true. rn_hmin=-10 rn_e3zps_min=25 rn_e3zps_rat=0.2	Use z-coordinate with partial bottom cells. Minimum number of ocean levels equals 10. Partial cell thickness is more than 25 m or more than 0.2 x layer thickness if the result is less than 25m.
rn_rdt = 200 rn_baro = 100 rn_atfp = 0.1	Baroclinic time step is 200 s. 100 Barotropic timesteps per baroclinic timestep. Asselin time filter parameter.
rn_fsbc=1 ln_blk_core=.true. nn_ice=2 ln_dm2dc=.true. ln_rnf=.true. nn_fwb=3	Surface boundary condition calculated each timestep. Use CORE bulk formulation for surface boundary condition. Use ice model. Convert mean downward short wave to a daily cycle. Land runoff included. Global freshwater budget set to zero by adding/subtracting constant over ocean.
ln_traqsr=.true. ln_qsr_2bd=.true. rn_abs=0.58 rn_si0=0.35 rn_si1=23.0	Downward light (short radiation) penetrates ocean surface. Downward radiation processed as two bands. Fraction of downward radiation entering ocean. Extinction depth (m) for long downward radiation. Extinction depth (m) for short downward radiation.
ln_rnf_mouth=.true. rn_hrnf=10.0 rn_avt_rnf=2.0 10 ⁻³ rn_rfact=1.02	Runoff defined at river mouths. Depth for enhanced vertical mixing in runoff areas. Additional mixing coefficient [$m^2 s^{-1}$]. Multiplicative factor for runoff.
ln_ref_apr=.false. nn_ssr=2 rn_deds=-33.333 ln_ssr_bnd=.true. rn_ssr_bnd=4.0	Model not forced by atmospheric pressure. Ocean surface layer salinity restored to climatology. Restoring term for salinity [$W m^{-2} / psu$] Limit absolute magnitude of restoring term. Value of limit.
rn_cloud=0.06 rn_albice=0.53 rm_alphd = 0.80 rm_alphc = 0.65 rm_alphdi=0.72	Cloud correction to snow and ice albedo. Albedo of melting ice in Arctic and Antarctic. Coefficients used to compute albedo between two extremes. (Payne 1972).
rn_shlat = 0	Momentum equation uses free slip boundary condition on sidewalls.
nn_bfr=2 rn_bfri2 = 1.0 10 ⁻³ rn_bfeb2 = 2.5 10 ⁻³ nn_bbl_ldf=1 nn_bbl_adv=0 rn_ahtbbl=1000	Non-linear bottom friction term. Non-linear bottom drag coefficient. Background turbulent kinetic energy near bottom [$m^2 s^{-2}$]. Diffusive bottom boundary layer. No advective bottom boundary layer. Lateral mixing coefficient in the bottom boundary layer.
nn_eos	UNESCO equation of state (Jackett and McDougall (1994)).
ln_traadv_tvd = .true. ln_traldf_lap=.true.	TVD advection scheme for tracers. Laplacial horizontal diffusion for tracers.

ln_trldf_iso=.true. rn_aht_0=125.0	Horizontal diffusion along iso-neutral surfaces. Horizontal diffusion coefficient for tracers [m^2s^{-1}].
nn_hdmp=-1 nn_zdmp =0 rn_surf=50.0 rn_bot=360.0 rn_dep=800.0	Relaxation of temperature and salinity towards Levitus in Red Sea and Mediterranean throughout water column. Surface relaxation time scale [days]. Bottom relaxation time scale [days]. Transition depth between surface and bottom term [m.].
ln_dynadv_cec = .true. ln_dybvor_eeen = .true.	Vector form of momentum advection. Entropy and energy conserving form of scheme.
ln_dynldf_bilap=.true. rn_ahm_0_blp=-1.25 10 ¹⁰	Bi-Laplacian horizontal diffusion of momentum. Bi-Laplacian coefficient.
rn_avm0 = 1.0 10 ⁻⁴ rn_avt0 = 1.0 10 ⁻⁵ ln_zdfevd=.true. nn_evdm=.true. rn_avevd=10.0	Background vertical viscosity (momentum) [m^2s^{-1}]. Background vertical diffusivity (tracers) [m^2s^{-1}]. Enhanced vertical diffusion (EVD). EVD applied to tracers only. EVD Coefficient [m^2s^{-1}].
rn_ediff = 0.1 rn_ediss = 0.7 rn_ebb = 60.0 rn_emin = 1.0 10 ⁻⁶ rn_emin0= 1.0 10 ⁻⁴ rn_mxl=3	Coefficient for vertical diffusion of eddy energy. Coefficient of Colmogoroff dissipation. Coefficient for surface input of TKE. Minimum value of TKE [m^2s^{-2}]. Surface minimum value of TKE [m^2s^{-2}]. Mixing length equals first vertical derivative of mixing length with a distinct dissipative and mixing length scale.
nn_pdl=1 ln_mx10=.true. rn_mx10=0.01 ln_lc=.true. rn_lc=0.15 nn_etau=1 rnEFR=0.05 nn_htau=1	Prandtl number is a function of the Richardson number. Surface mixing length scale is a function of the wind stress. Minimum value of surface buoyancy length scale. Parameterisation of Langmur Cells (Axell 2002). Langmur cell coefficient. TKE penetrates below the mixed layer due to internal and inertial waves. Fraction of surface TKE value penetrating below the mixed layer. TKE scheme with Rodgers et al. (2014) mixing length scheme.

Appendix 2. CORE Surface Flux Terms

The CORE Surface Flux terms are the ones proposed by Large and Yeager (2004). In the NEMO model, the corresponding computer code is in subroutines 'blk_oce_core' and 'turb_core_2z' of file 'sbcbulk_core.F90'.

The atmospheric data used to force the model is from the Drakkar forcing datasets. These are based on ECMWF reanalysis data. Run 1 uses DFS4.1, described in Brodeau et al. (2010). Run 6 uses DFS5.2, described in Dussin et al. (2014). The atmospheric variables used to calculate the surface fluxes are,

T_a	Air Temperature at 2 m. ($^{\circ}C$)
H_a	Specific Humidity at 2 m. (kg/kg)
U_a	Wind (east component) at 10 m. (ms^{-1})
V_a	Wind (north component) at 10 m. (ms^{-1})
F_{ss}	Short Wave Flux (Downward) (Wm^{-2})
F_{la}	Long Wave Flux (Downward) (Wm^{-2})

The model variables used are the ocean sea surface temperature T_o and the components of the surface current U_o and V_o . Then defining,

U	$= ((U_a - U_o)^2 + (V_a - V_o)^2)^{1/2}$	Air speed relative to ocean surface
α	$= 0.066$	Ocean albedo
Υ	$= 5.6710^{-8}$	Stephan-Boltzmann Constant
ρ_a	$= 1.22$	Density of air
ζ	$= 1000.5$	Specific heat of air
F_{lo}	$= \Upsilon T_o^4$	Long Wave Flux out of Ocean
Z_c	$= 0.98 * 640380 / \rho_a$	Saturation Coefficient
Z	$= Z_c \exp(-5107.4/T_o)$	Specific Humidity of Saturated Air at temperature T_o

The surface transfer coefficients for heat C_h and evaporation C_e , depend on the atmospheric stability and are calculated by routine 'turb_core_2z'. The fluxes are then,

F_{sw}	$= (1 - \alpha)S$	Short Wave Flux into Ocean
F_{lw}	$= F_{lo} - F_{la}$	Net Long Wave Flux out of Ocean
F_h	$= \rho_a \zeta C_h U_r (T_o - T_a)$	Sensible Heat Flux out of Ocean
E	$= \rho_a C_e U (Z - H_a)$	Evaporation
F_e	$= L_v E$	Latent Heat Flux out of Ocean

References

- Arakawa, A.: Computational design for long-term numerical integration of the equations of fluid motion: Two-dimensional incompressible flow, *Journal of Computational Physics*, 1, 119–143, 1966.
- Brodeau, L., Barnier, B., Treguier, A.-M., Penduff, T., and Gulev, S.: An ERA40 based atmospheric forcing for global ocean circulation models, *Ocean Modelling*, 31, 88–104, 2010.
- Dussin, R., Barnier, B., and Brodeau, L.: The making of Drakkar forcing set DFS5, Report 05-10-14, DRAKKAR/MyOcean, 2014.
- Gaspar, P., Gregoris, Y., and Lefevre, J.-M.: A simple eddy kinetic energy model for simulations of the oceanic vertical mixing: Tests at station Papa and long-term upper ocean study site, *Journal of Geophysical Research*, 95 (C9), 16 179–16 193, doi:10.1029/JC095iC09p16179, 1990.
- Hirahara, S., Ishii, M., and Fukuda, Y.: Centennial-scale sea surface temperature analysis and its uncertainty, *Journal of Climate*, 27, 57–75, 2014.
- Huang, B., Banzon, V. F., Freeman, E., Lawrimore, J., Liu, W., Peterson, T. C., Smith, T. M., Thorne, P. W., Woodruff, S. D., and Zhang, H.-M.: Extended Reconstructed Sea Surface Temperature Version 4 (ERSST.v4). Part I: Upgrades and Intercomparisons, *Journal of Climate*, 28, 911–930, doi:10.1175/JCLI-D-14-00006.1, 2015.
- Large, W. and Yeager, S.: Diurnal to Decadal Global Forcing for Ocean and Sea-Ice Models: The Data Sets and Flux Climatologies, NCAR Technical Note TN-460+STR, National Centre for Atmospheric Research, Boulder, Colorado, 2004.
- Liu, W., Huang, B., Thorne, P. W., Banzon, V. F., Zhang, H.-M., Freeman, E., Lawrimore, J., Peterson, T. C., Smith, T. M., and Woodruff, S. D.: Extended Reconstructed Sea Surface Temperature Version 4 (ERSST.v4): Part II. Parametric and Structural Uncertainty Estimations, *Journal of Climate*, 28, 931–951, doi:10.1175/JCLI-D-14-00007.1, 2015.
- Madec, G.: NEMO ocean engine (Draft edition r6039), Note du Pole de modelisation 27, Institut Pierre-Simon Laplace (IPSL), France, 2014.
- Merchant, C., Embury, O., Rayner, N., Berry, D., Corlett, G., Lean, K., Veal, K., Kent, E., Llewellyn-Jones, D., Remedios, J., and Saunders, R.: A 20 year independent record of sea surface temperature for climate from Along Track Scanning Radiometers, *Journal of Geophysical Research*, 117(C12013), 931–951, doi: 10.1029/2012JC008400, 2015.
- Rayner, N. A., Parker, D. E., Horton, E. B., Folland, C. K., Alexander, L. V., Rowell, D. P., Kent, E. C., and Kaplan, A.: Global analyses of sea surface temperature, sea ice, and night marine air temperature since the late nineteenth century, *Journal of Geophysical Research*, 108(14), doi:10.1029/2002JD002670, 2003.
- Rodgers, K., Aumont, O., Mikaloff Fletcher, S., Plancherel, Y., Bopp, L., de Boyer Montgut, C., Iudicone, D., Keeling, R., Madec, G., and Wanninkhof, R.: Strong sensitivity of Southern Ocean carbon uptake and nutrient cycling to wind stirring, *Biogeosciences*, 11(15), 4077–4098 doi=10.5194/bg-11-4077-2014, 2014.
- Trenberth, K. E.: The Definition of El Nino, *Bulletin of the American Meteorological Society*, 78, 2771–2777, doi:10.1175/1520-0477(1997)078<2771:TDOENO>2.0.CO;2, 1997.
- Wyrtki, K.: El Nino - the dynamic response of the Equatorial Pacific ocean to atmospheric forcing, *Journal of Physical Oceanography*, 5, 572–584, 1975.
- Zalesak, S.: Fully multidimensional flux corrected transport algorithms for fluids, *Journal of Computational*

Physics, 31, 335–362, 1979.